

1
2
3
4
5
6
7
8
9
10
11
12
13
14
15
16
17
18
19
20
21
22
23
24
25
26
27
28

Supplementary materials for

**Impact of urbanization on mesoscale convective systems:
insights from a radar wind profiler MESONET, theoretical
analyses, and model simulations**

Tian Xian¹, Jianping Guo^{2*}, Runze Zhao³, Xiaoran Guo², Ning Li², Yuping Sun²,
Zhen Zhang², Tianning Su⁴, Zhanqing Li^{4*}

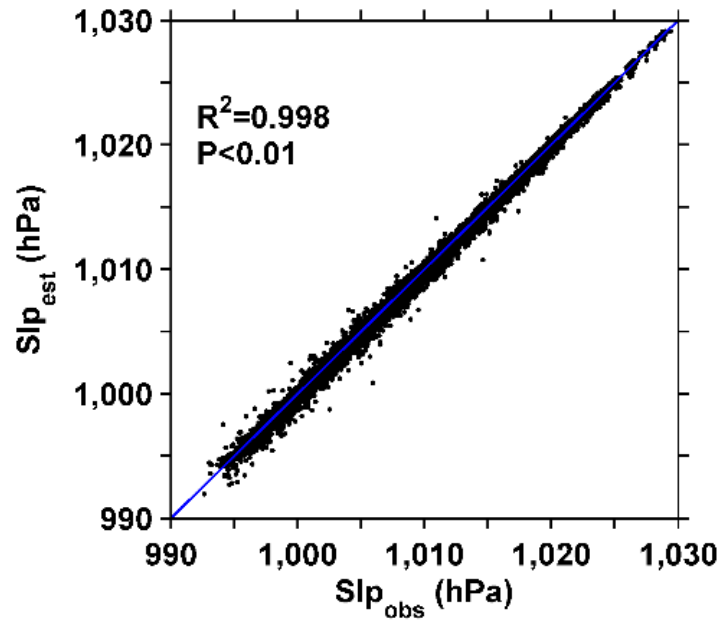
¹ State Key Laboratory of Remote Sensing Science, College of Global Change and
Earth System Science, Beijing Normal University, Beijing 100875, China

² State Key Laboratory of Severe Weather, Chinese Academy of Meteorological
Sciences, Beijing 100081, China

³ National Satellite Meteorological Center (National Center for Space Weather),
China Meteorological Administration, Beijing, 100081, China

⁴ Dept. of Atmos. & Oceanic Sci. and ESSIC, University of Maryland, College Park,
Maryland 20740, United States

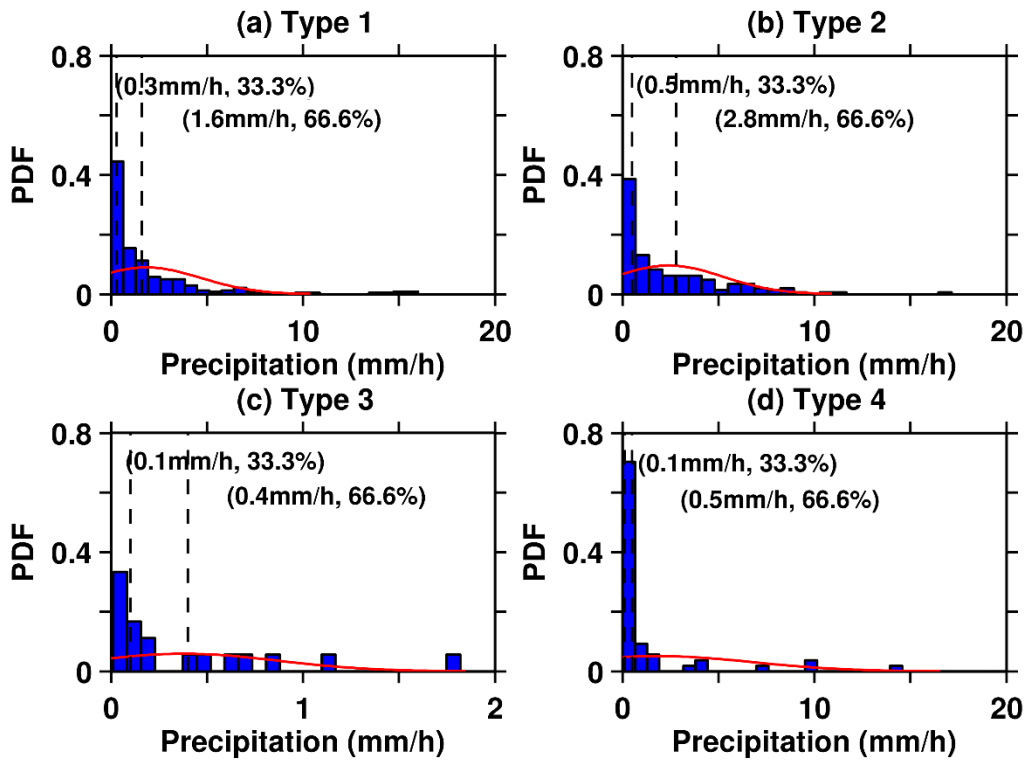
*Correspondence to: Dr./Prof. Zhanqing Li (Email: zli@atmos.umd.edu)
and Dr./Prof. Jianping Guo (Email: jpguocams@gmail.com)



29

30 **Figure S1.** Scatter plot of the estimated daily sea level pressure (Slp_{est}) against observed
31 sea level pressure (Slp_{obs}).

32



33

34

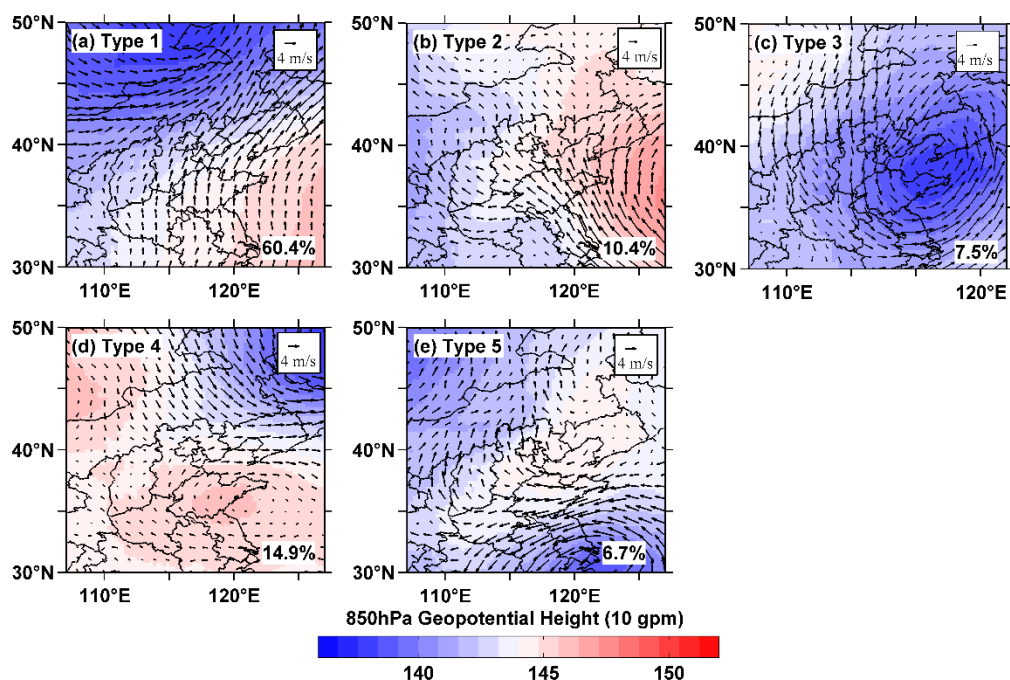
Figure S2. Frequency distribution of the precipitation produced by MCS under different synoptic types.

35

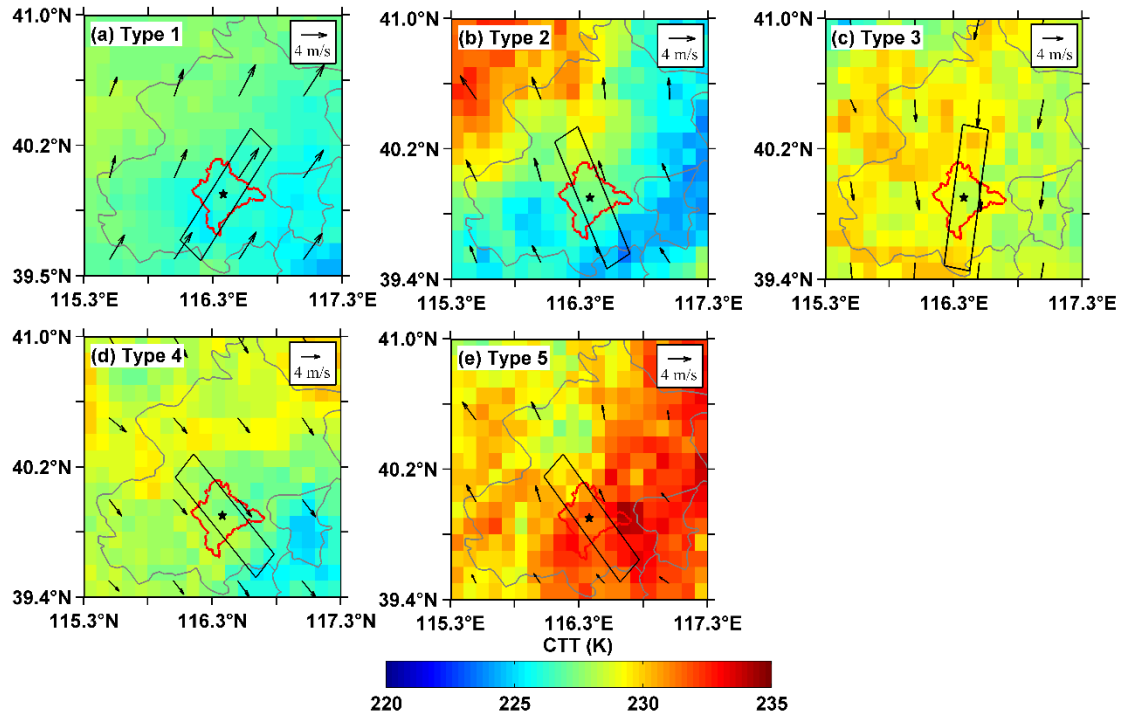
36

37 To test whether the number of principal components exerts influences on the
 38 classification of atmospheric circulation, we conducted sensitivity analysis by applying
 39 the number of principal components of 5. Similarly, Figure S3 shows the five dominant
 40 synoptic patterns under which all MCS events occurred in Beijing during the warm
 41 season (from May to September) of 2018–2019. For the classification results with a
 42 principal component fraction of 5, the first three circulation patterns are strong synoptic
 43 forcing, while the last two circulation patterns are weak synoptic forcing. Type 1
 44 Beijing is located on the periphery of the western Pacific subtropical high, consistent
 45 with Type 1 in Fig.4. Type 2 Beijing is controlled by the strong high-pressure system
 46 in the east, similar to the "high pressure in the east and low pressure in the west" pattern.
 47 Under this circulation, the southerly wind dominates the region, and bringing warm and
 48 humid air masses that are conducive to the occurrence of MCS. Type 3 is in front of the
 49 cold front and is more likely to generate MCS near the cold front. Under Type 4 and
 50 Type 5, the Beijing area is respectively controlled by high pressure and uniform
 51 pressure fields, and the generation of MCS tends to be more influenced by local factors.

52 For the evolution of CTT (Fig. S4-S5), with a number of principal components of
 53 5, when dominated by strong (weak) forcing, the average CTT along the urban
 54 prevailing wind also shows a significant upward (downward) trend. Which indicates
 55 that the number of principal components does not significantly affect the conclusions.

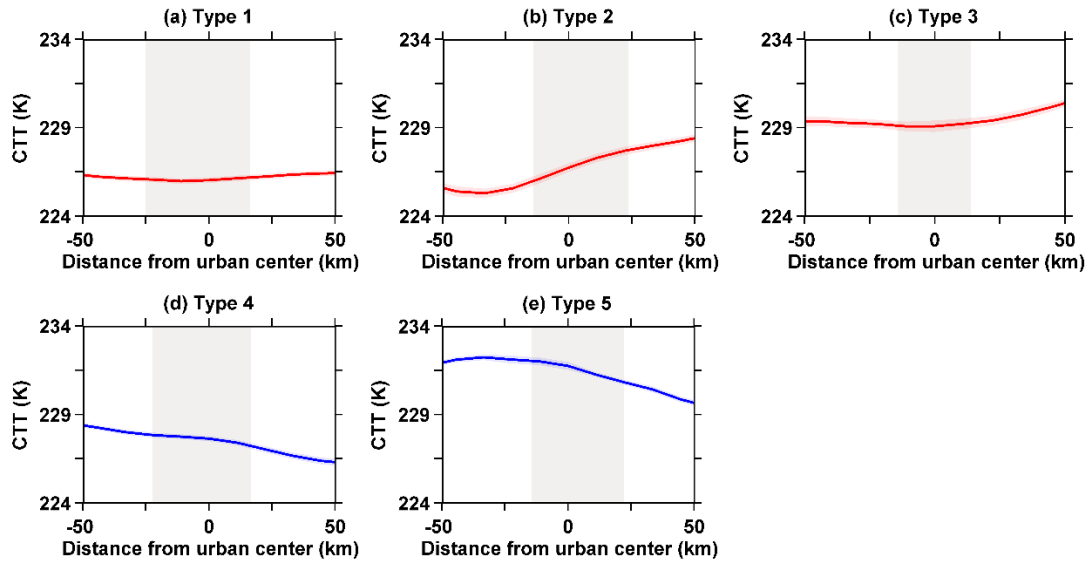


56
 57 **Figure S3.** Five dominant synoptic patterns showing the field of 850-hPa geopotential
 58 height (color shading) superimposed by the wind field at 850-hPa (arrow) linked to the
 59 MCS events occurring in Beijing during the warm season (from May to September) of
 60 2018–2019, which are derived from ERA-5 reanalysis using the T-PCA classification
 61 method.
 62



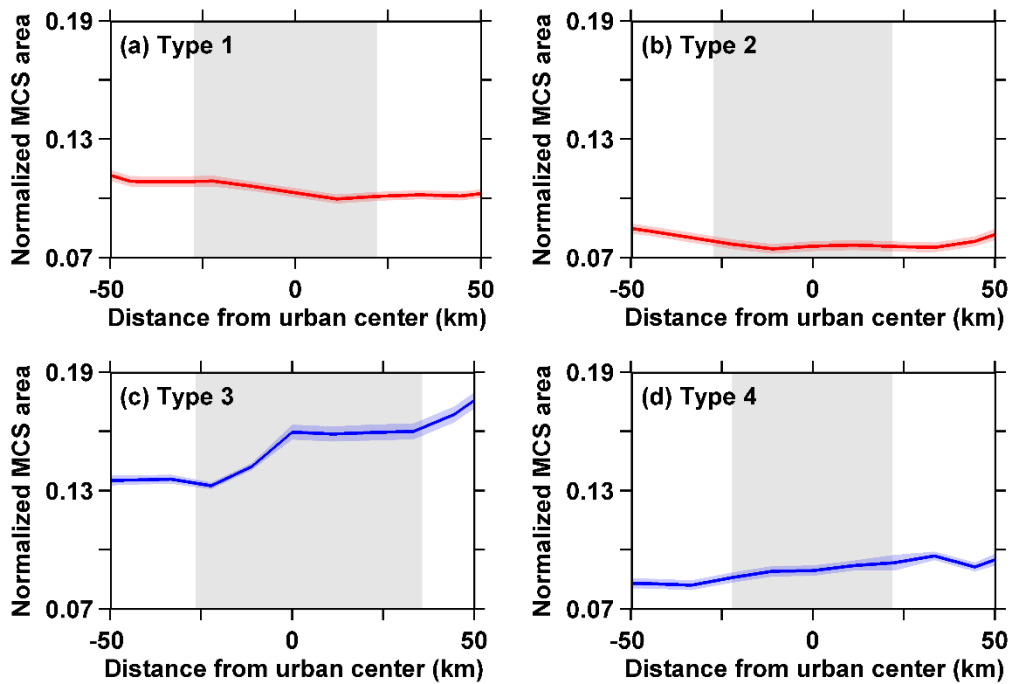
63
 64
 65
 66
 67
 68

Figure S4. Spatial distribution of CTT from the FY-2 geostationary satellite for the five synoptic patterns. Red polygon outlines the urban area of Beijing, and the black rectangle (100 km × 20 km) is used to describe the spatial gradient of CTT centered on the Beijing urban area under the prevailing wind for each synoptic pattern.



69

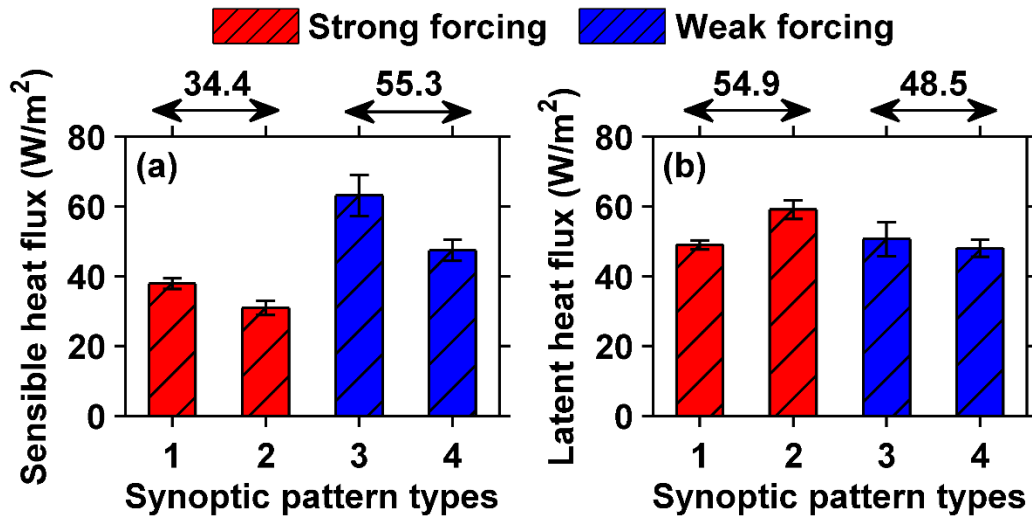
70 **Figure S5.** Spatial evolution of satellite-observed cloud-top temperature (CTT, solid
 71 line) as calculated for all the MCS samples that are located at one given location along
 72 the prevailing wind in the black rectangles shown in Fig. S4 for the five different
 73 synoptic patterns: Type 1 (a), Type 2 (b), Type 3 (c), Type 4 (d) and Type 5 (e). The
 74 grey shading represents the urban area.
 75



76

77 **Figure S6.** Spatial evolution of normalized MCS area along the prevailing wind in the
 78 black rectangles shown in Fig. 5 for the four different synoptic patterns: Type 1 (a),
 79 Type 2 (b), Type 3 (c), and Type 4 (d). The grey shading represents the urban area, and
 80 the normalized MCS area at one given location refers to the cloud area in this location
 81 divided by its total area throughout its entire life cycle. The grey shading represents the
 82 urban area.

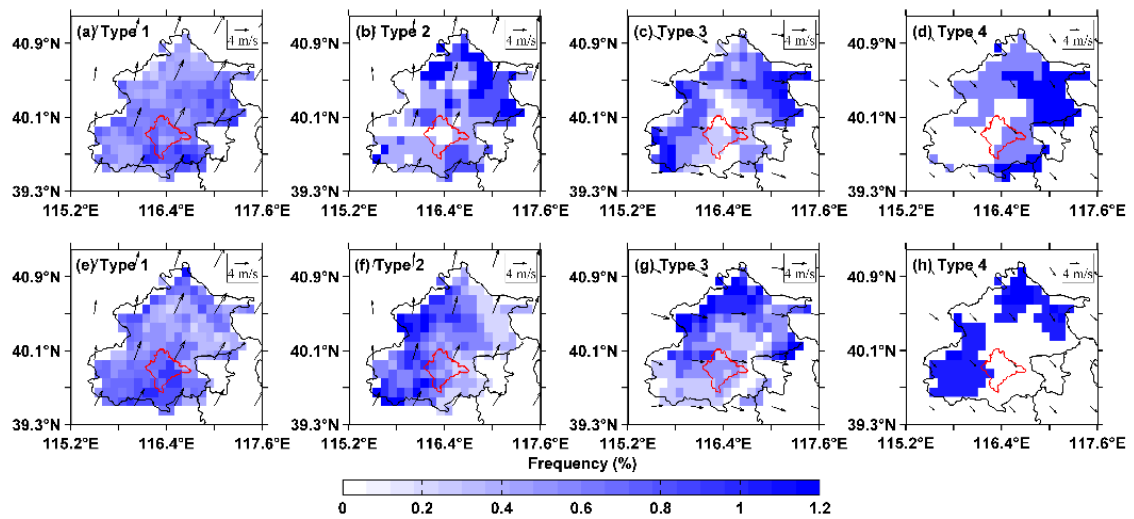
83



84

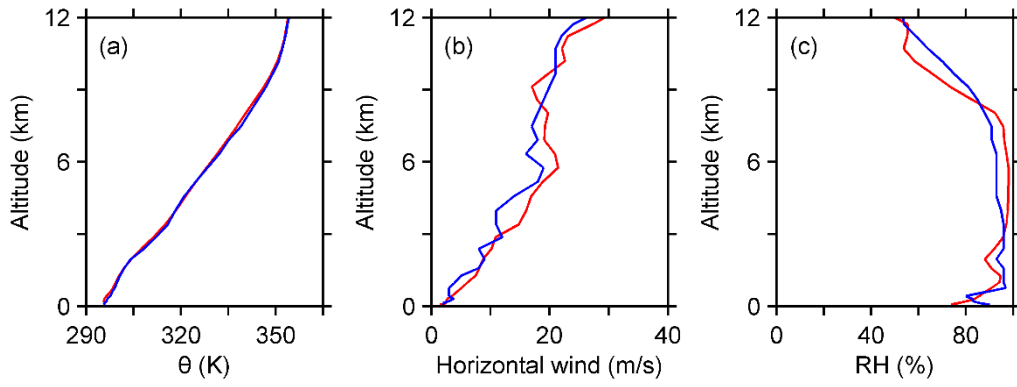
85 **Figure S7.** (a) Surface sensible heat flux (unit: W/m^2), and (b) Surface latent heat flux
 86 (W/m^2) for different synoptic pattern types. The red (blue) bars for strong (weak)
 87 forcing denote the results of types 1, 2 (types 3, 4) and the values above the figure
 88 represent the results of the combined average of strong (weak) forcing.

89



90
91
92
93
94
95

Figure S8. Spatial distribution of the occurrence frequency of MCS (a-d) initiation and (e-h) dissipation as calculated from the warm season (May-September for the period 2018-2019) observations in Beijing under type 1 (a, e), type 2 (b, f), type 3 (c, g), and type 4 (d, h) synoptic pattern. The red polygon refers to the Beijing metropolitan area.

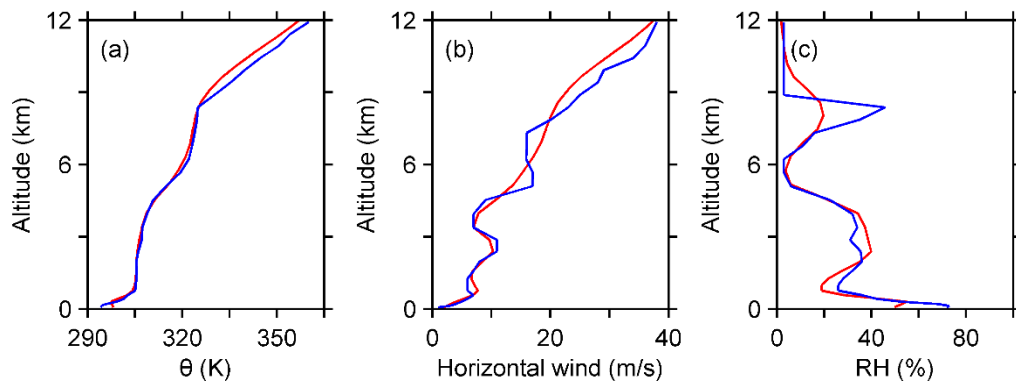


96

97 **Figure S9.** Simulated (a) θ , (b) horizontal wind and (c) RH by WRF-LES (blue lines)
 98 under strong synoptic forcing and the corresponding observation by soundings (red
 99 lines) at 0800 LST on 11 July 2018.

100

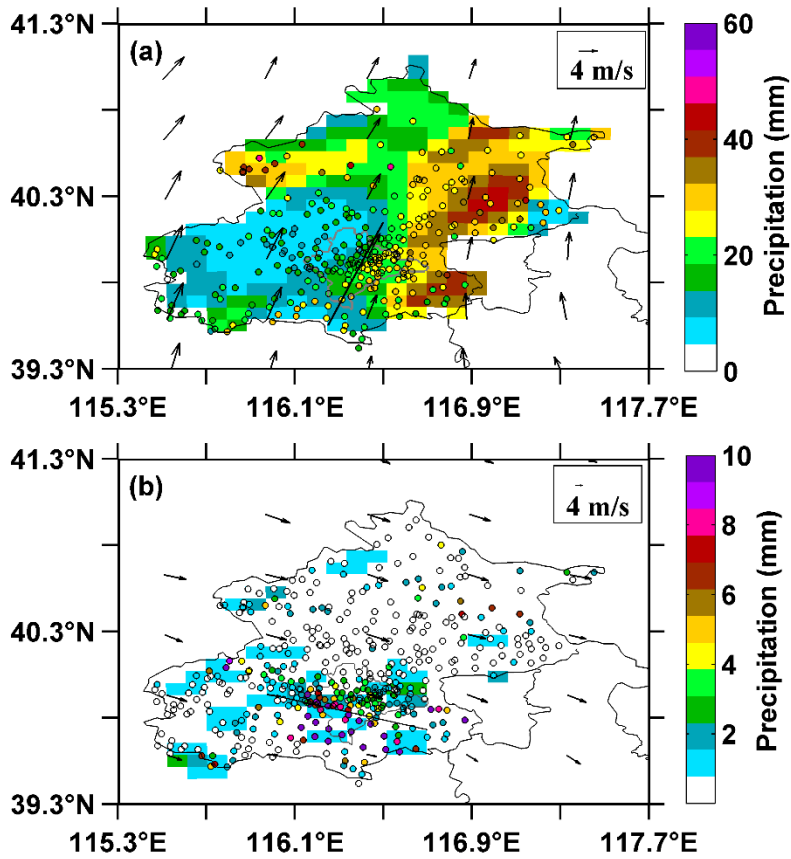
101



102

103 **Figure S10.** Simulated (a) θ , (b) horizontal wind and (c) RH by WRF-LES (blue lines)
104 and the corresponding observation by soundings (red lines) at 0800 LST on 1
105 September 2020, when a weak synoptic pattern dominated the study area.

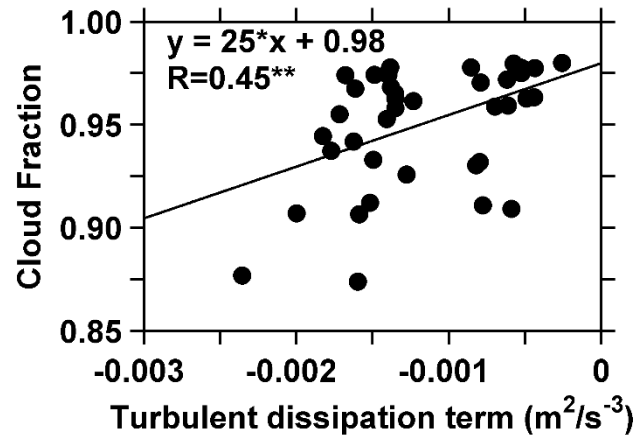
106



107

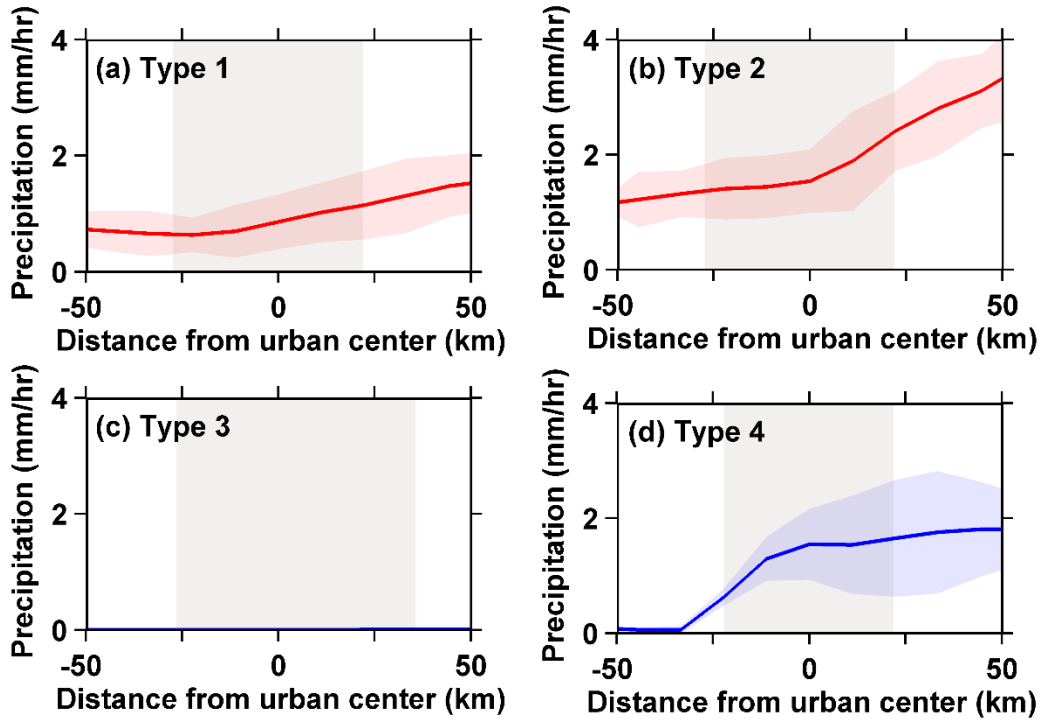
108 **Figure S11.** The spatial distributions of cumulative precipitation amount from WRF-
 109 LES simulations (color-shaded area) and observations (color-shaded dots) at (a) 20:00
 110 BJT on 10 July to 20:00 BJT on 11 July 2018 and (b) 20:00 BJT on 31 August to 20:00
 111 BJT on 1 September 2020.

112



113

114 **Figure S12.** Relationship between the turbulent dissipation term and the cloud cover
 115 under strong precipitating cases. The black solid line is the linear regression, and the
 116 superscript ** for R indicates that the regression slope is statistically significant
 117 at $p < 0.01$. The turbulent dissipation term represents the dissipation of TKE, where a
 118 smaller negative value indicates a larger dissipation of TKE.
 119



120

121

Figure S13. Same as Fig. S6, but for the precipitation produced by MCS.